



Effect of barium on LSGM electrolyte prepared by fast combustion method for solid oxide fuel cells (SOFC)

Erwin Sepúlveda¹ · Ramalinga Viswanathan Mangalaraja^{1,2} · Loreto Troncoso³ · José Jiménez⁴ · Christopher Salvo⁵ · Felipe Sanhueza¹

Received: 9 September 2022 / Accepted: 27 October 2022 / Published online: 7 November 2022
© The Author(s), under exclusive licence to The Materials Research Society 2022

Abstract

In this work, $\text{La}_{0.85}\text{Sr}_{0.15-x}\text{Ba}_x\text{Ga}_{0.85}\text{Mg}_{0.15}\text{O}_{3-\delta}$ (LSBGM), with $0 \leq x \leq 0.075$, were prepared as electrolytes for solid oxide fuel cells applications. The effect of barium and sintering temperature on the structure and electrical properties was studied. A fast combustion method was used, starting with nitrate salts and citric acid as fuel. The XRD spectra showed two main phases corresponding to LSGM orthorhombic (space group Imma) and LSGM-cubic (space group Pm-3 m). From literature, both structures are reported as high oxygen ion conductive species, but normally, they are not reported to appear together. Major secondary phases were LaSrGaO_4 , BaLaGaO_4 , and BaLaGaO_7 . SEM revealed a material with low porosity, indicating incomplete densification. The sample $\text{La}_{0.85}\text{Sr}_{0.075}\text{Ba}_{0.075}\text{Ga}_{0.85}\text{Mg}_{0.15}\text{O}_{3-\delta}$ showed a conductivity of 0.016 and 0.058 S cm^{-1} at 600 °C and 800 °C, respectively. This means an improvement of 34% compared to the non-barium sample $\text{La}_{0.85}\text{Sr}_{0.15}\text{Ga}_{0.85}\text{Mg}_{0.15}\text{O}_{3-\delta}$ at 600 °C. Thus, this composition could be used in SOFC.

Introduction

As is well known, the CO_2 concentrations in the atmosphere have skyrocketed in recent decades, reaching more than 418 ppm [1]. This is often associated with climate change and subsequent problems. Fuel cells emerged as

a clean alternative to produce energy through an electrochemical reaction CO_2 -free. Typical fuels are CH_4 , CO, and CO_2 [2]. The solid oxide fuel cell (SOFC) tends to have the highest efficiencies [3]. A typical SOFC consists of a solid electrolyte, a fuel electrode, and the air/oxygen electrode. Classical electrolytes are ceria and zirconia with excellent performance near 800 – 1000 °C, some degradation may occur, besides the high fabrication cost for the device to operate at these temperatures. To face this inconvenience, LaGaO_3 -based materials have become a good option. They show high ionic conduction under both oxidant and reducing atmosphere [4] and good thermal and chemical stability [5] at a lower temperature (600 – 800 °C). The intermediate working temperature for fuel cells allows cost-effective gas sealing and interconnecting materials [6].

Structural modification of LaGaO_3 (general formula ABO_3) by the introduction of dopants both in positions A and B allows an increase in the O_2 due to the creation of oxygen defects in the LaGaO_3 perovskite [7]. Thus, the ionic conductivity increases, improving the whole performance of the fuel cell. One traditional dopant is Sr for position A, while Mg is studied for position B leading to the classic LSGM structure [5]. Huang and Goodenough [8] reported a contour diagram for the optimum composition of LSGM by varying the strontium (x : 0.1–0.2) and magnesium (y : 0.1–0.2) content. In low concentrations, some codopants such as Ca have

✉ Erwin Sepúlveda
ersepulveda@udec.cl

✉ Ramalinga Viswanathan Mangalaraja
mangal@udec.cl

¹ Advanced Ceramics and Nanotechnology Laboratory, Department of Materials Engineering, Faculty of Engineering, University of Concepcion, 4070409 Concepción, Chile

² Faculty of Engineering and Sciences, Universidad Adolfo Ibáñez, Diagonal Las Torres 2640, Santiago, Peñalolén, Chile

³ Institute of Materials and Thermomechanics, Universidad Austral de Chile, General Lagos 2086, 5111187 Valdivia, Chile

⁴ Materialia Group—Physical Metallurgy Department, National Centre for Metallurgical Research (CENIM-CSIC), Av. de Gregorio del Amo, 8, 28040 Madrid, Spain

⁵ Departamento de Ingeniería Mecánica, Facultad de Ingeniería, Universidad del Bío-Bío, 4030000 Concepción, Chile

been studied [4]. Biswal and Biswas [9] found that the presence of barium as codopant at 5% increased the conductivity of $\text{La}_{0.85}\text{Sr}_{0.1}\text{Ba}_{0.05}\text{Ga}_{0.85}\text{Mg}_{0.15}\text{O}_{3-\delta}$ by 44% (0.046 S cm^{-1} @600 °C) concerning non-barium electrolyte. Singh [10] found that a barium content of 0.07% increased the conductivity, but higher concentrations made the conductivity worst.

Besides the chemical composition, the crystal structure is decisive for oxygen diffusion: cubic and orthorhombic facilitate this mechanism for LaGaO_3 -based electrolytes [11]. Typically, researchers report one of these phases at once but it is rare to find the coexistence of both of them. For example, Wang et al. [12] mention that the crystal structure of undoped LaGaO_3 is orthorhombic at room temperature, while Huang et al. [13] identified the cubic phase as the main phase starting from oxides. Also, the differentiation of the phases is a matter of broad debate in the literature [11]. Then, the synthesis method has some relationship with the final structure and the electrical properties. A classical synthesis method is the solid-state reaction (SSR) which allows reaching high conductivity, with the inconvenience of being high time and energy consuming. Also, techniques such as sol-gel [14], Pechini, and the use of organic fuels such as ethylenediaminetetraacetic acid (EDTA), citric acid (CA), polyvinyl alcohol (PVA), and tartaric acid (TA) [15] are used to reach pure phases. For instance, the Pechini method involves the formation of stable metal-chelate complexes with specific alpha hydroxy carboxyl acids, such as citric acid (CA), and the poly esterification in the presence of polyhydroxy alcohol, such as ethylene glycol (EG), to form a polymeric resin. Thus, metal cations are better distributed among the resin, which aids the obtention of a homogeneous material after calcination [16]. This method is suitable for preparing multi-component oxides of high purity at low temperatures [17, 18]. The pure phase of LSGM normally appears between 1400 and 1450 °C [19] and frequent secondary phases are $\text{SrLaGa}_3\text{O}_7$ and SrLaGaO_4 [20].

In this work, a LaGaO_3 -based electrolyte was synthesized by the fast combustion method. The idea is based on reaching the maximum conductivity using a shorter and less energetically expensive method than some studied until now. The effect of the barium content as codopant in position A

and the sintering temperature on the final properties was investigated.

Methodology

The fast combustion method was used to synthesize the $\text{La}_{0.85}\text{Sr}_{1-x}\text{Ba}_x\text{Ga}_{0.85}\text{Mg}_{0.15}\text{O}_{3-\delta}$ (LSBGM) with $x = 0; 0.05; 0.075$. Nitrate salts as starting materials were put into a beaker glass. The citric acid (CA) was added as fuel and distilled water. The mixture was stirred for 10 min and then burnt in a furnace to complete the fast combustion method. The precursors and purity are provided in Table 1. For a typical preparation, a selected amount of nitrates was mixed with citric acid (CA) at a molar ratio CA/nitrates of 2. Nitrate salts were used for their high solubility at room temperature. Distilled water was added and subjected to stirring for 15 min at 500 rpm at room temperature. The solution was then transferred to an alumina crucible and subjected to heat treatment in an oven (Muffle Nabertherm, LT) at 500 °C for 10 min to achieve the full combustion reaction. The resultant foamy material was carefully collected and ground into powder using an agate mortar. The as-prepared fine powder was stored in hermetic vessels until further heat treatment. The as-prepared powder was then subjected to calcination at 1000 °C for 4 h with a heating and cooling rate of 8 °C/min (hereby referred to as calcinated powder). A color change in the powder from black to light brown was evident. The brown powder was then molded into pellets using a uniaxial pressing with 10,000 lb_f for 1 min at room temperature. The pellets were then subjected to sintering at 1400 °C and 1450 °C for 6 h. (ramp ≈ 5.7 °C/min) using a muffle furnace (Nabertherm HT 16/16). The sintering temperature and barium content were studied on the final properties of the LSBGM electrolyte. Samples are code named as given in Table 2.

X-ray diffractograms for the samples in the range of 20–80° were obtained using a (Bruker AXS, D4 Endeavor, Bremen, Germany) with 40 kV, 20 mA, and 0.1542 nm Cu-K α line. Rietveld refinements for phase quantification and further microstructural information were made by software TOPAS-Brucker. The morphology change

Table 1 Starting materials used for the preparation of the LSGM

Precursor	Formula	Purity %	Vendor
Lanthanum (III) nitrate hexahydrate	$\text{La}(\text{NO}_3)_3 \cdot 6\text{H}_2\text{O}$	99.999	Merck
Strontium nitrate	$\text{Sr}(\text{NO}_3)_2$	≥ 99	Sigma Aldrich
Gallium (III) nitrate hydrate	$\text{Ga}(\text{NO}_3)_3 \cdot x\text{H}_2\text{O}$	99.9	Sigma Aldrich
Magnesium nitrate hexahydrate	$\text{Mg}(\text{NO}_3)_2 \cdot 6\text{H}_2\text{O}$	99.0	Sigma Aldrich
Barium Nitrate	$\text{Ba}(\text{NO}_3)_2$	≥ 99	Sigma Aldrich
Citric acid (CA)	$\text{C}_6\text{H}_8\text{O}_7$	99.0	Sigma Aldrich
Distilled water (DW)	H_2O	–	Diprolab

Table 2 Variation of the composition in samples with code names

Theoretical composition sintered at 1400 °C	Code name	Theoretical composition sintered at 1450 °C	Code name
$\text{La}_{0.85}\text{Sr}_{0.15}\text{Ga}_{0.85}\text{Mg}_{0.15}\text{O}_{3-\delta}$	A1	$\text{La}_{0.85}\text{Sr}_{0.15}\text{Ga}_{0.85}\text{Mg}_{0.15}\text{O}_{3-\delta}$	B1
$\text{La}_{0.85}\text{Sr}_{0.10}\text{Ba}_{0.05}\text{Ga}_{0.85}\text{Mg}_{0.15}\text{O}_{3-\delta}$	A2	$\text{La}_{0.85}\text{Sr}_{0.10}\text{Ba}_{0.05}\text{Ga}_{0.85}\text{Mg}_{0.15}\text{O}_{3-\delta}$	B2
$\text{La}_{0.85}\text{Sr}_{0.075}\text{Ba}_{0.075}\text{Ga}_{0.85}\text{Mg}_{0.15}\text{O}_{3-\delta}$	A3	$\text{La}_{0.85}\text{Sr}_{0.075}\text{Ba}_{0.075}\text{Ga}_{0.85}\text{Mg}_{0.15}\text{O}_{3-\delta}$	B3

was analyzed by SEM (JSM-6380LV, Chicago, IL, USA). For the SEM studies, the samples were pre-coated with gold film. Density was calculated using the Archimedes method. The mechanical microhardness at room temperature of the consolidated material was evaluated using an 8187.5 ZHU Zwick/Roell microhardness tester. The bulk microhardness of each sample was characterized by an average value taken from eight indentations carried out by applying a load of 3 N on a polished surface for 10 s at different locations. For the electrochemical impedance spectroscopy (EIS) studies, Bio-Logic BP-300 *potentiostat* system was adopted. For these studies, the pellets were coated with silver paste on both faces and allowed to cure at 200 °C for 2 h. The measurements were carried out in the frequency range of 6 MHz to 100 MHz for an amplitude of 50 mV. The measurements were carried out in an isolated alumina tube inside a furnace (Thermcraft XST-3-0-12-1V2). The impedance measurements were carried out under different temperatures (300–800 °C). The conductivity related to grain or grain boundary was calculated from the equation $\sigma_{g/gb} = L/(AR_{g/gb})$ where L is the thickness, A is the area, and R is the resistance for grain (R_g) or grain boundary (R_{gb}). The activation energy was obtained from the respective Arrhenius plot and Eq. 1.

$$\sigma = \left(\frac{A}{T}\right) \exp\left(-\frac{E_a}{kT}\right) \quad (1)$$

Results and discussion

X-ray diffraction (XRD)

XRD diffractograms for samples sintered at 1400 and 1450 °C are shown in Fig. 1. Corresponding Rietveld results are found in Table 3. For all samples, nine characteristic peaks of LSGM appeared between angles 20 and 80 °C. That indicates that the phase was formed, but almost negligible secondary phase peaks are also observed. For all samples, the main phase found was the orthorhombic LSGM with space group *Imma*, followed by a cubic LSGM phase (*Pm-3 m*). The crystalline structures present in the perovskite are very sensitive to slight variations in the dopants concentration, small local alterations of the exact stoichiometry can give rise to the appearance of different types of perovskites. For pellets sintered at 1450 °C, the cubic phase increases with the barium content. The secondary phase SrLaGaO_4 was common for both temperatures used, as well as the LSGM orthorhombic or cubic. BaLaGaO_4 , BaLaGaO_7 , and $\text{Ba}_{0.5}\text{Sr}_{0.5}\text{O}$ appeared for 1450 °C. BaLaGaO_4 has been reported by [21], while no reports for the other were

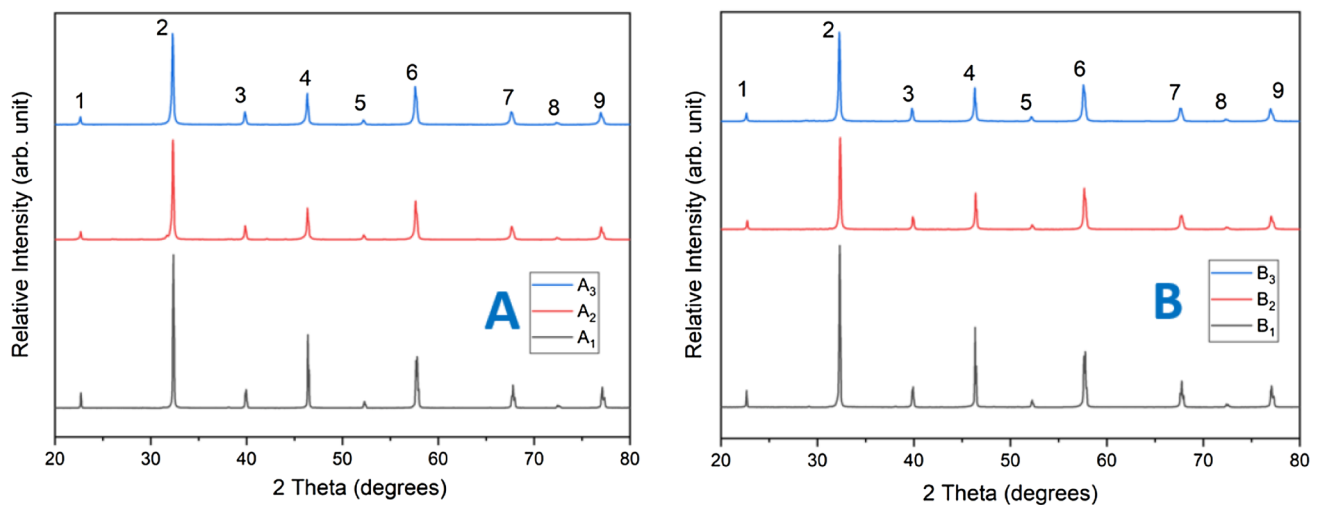
**Fig. 1** XRD for LSGM electrolyte sintered by 6 h at **A** 1400 °C and **B** 1450 °C

Table 3 Quantitative analysis for the current phases

Phase/Sample	1400 °C			1450 °C		
	A1	A2	A3	B1	B2	B3
LSGM (<i>Imma</i>)	96.6	77.64	86.88	89.59	85.37	85.2
LSGM (<i>Pm-3 m</i>)	2.5	8.96	13.12	9.96	11.78	13.11
SrLaGaO ₄ (<i>I4/mmm</i>)	0.95	–	–	0.45	1.425	–
BaLaGaO ₄ (<i>P212121</i>)	–	–	–	–	0.50	0.49
BaLaGaO ₇ (<i>P-421 m</i>)	–	–	–	–	0.85	1.05
Ba _{0.5} Sr _{0.5} O (<i>Fm-3 m</i>)	–	–	–	–	0.06	0.16
Others	–	13.39	–	–	–	–
LSGM (subtotal)	99.05	86.60	100.00	99.55	97.15	98.31

found. From Table 3, sample A1 showed the highest purity for the orthorhombic structure of LSGM at 1400 °C (96.59%). When the orthorhombic and cubic phases of LSGM are considered together, LSGM reached 100% at 1400 °C for samples A3.

Scanning electron microscopy (SEM)

The morphology of sintered pellets at 1400 °C and 1450 °C for 6 h was observed by SEM. Images are shown in Fig. 2. At first glance, almost negligible porosity is seen for samples sintered at 1400 °C. This indicates that the temperature and time of sintering are not enough to obtain a full densification. At 1400 °C, the pellet with a barium content of 7.5% (A3) presented a greater porosity.

Moreover, sample A2 exhibits a texture not observed in the other samples, associated with its higher quantity of secondary phases (up to 13.4%). On the other hand, the porous size observed at 1450 °C is nearly four times larger than the porous size at 1400 °C. This phenomenon is unusual at these temperatures: usually, the materials tend to be dense when temperature increases as an effect of sintering. Nevertheless, other studies reported similarities with this work [22].

Density and microhardness

The density, relative density, and microhardness are presented in Table 4. The values obtained are between 2 and 2.4 GPa, which are lower than the reported for similar materials (around 7 to 8 GPa) [23]. The samples appearance, mechanical properties, and porosity vary significantly with

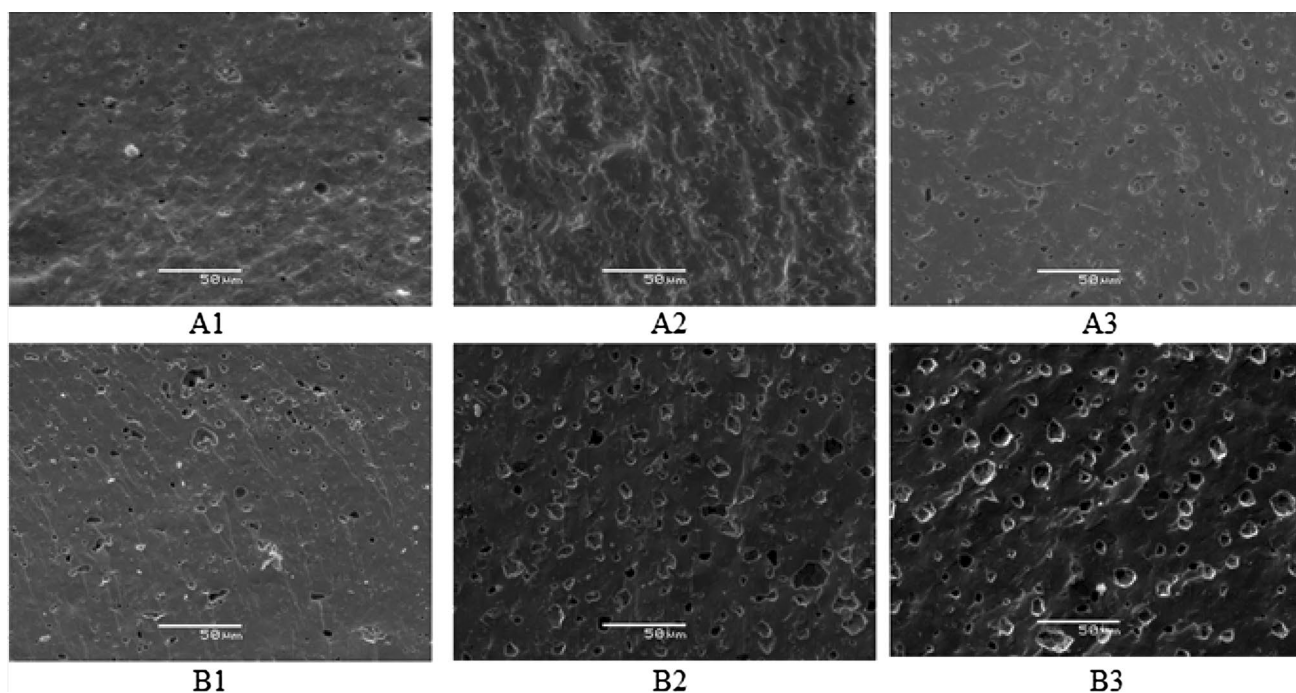


Fig. 2 Scanning electron microscopy images for different barium content and sintering temperature

Table 4 Properties of the electrolyte

Sample	Sintering Temp. (°C)	Microhardness (GPa)	Density (kg/m ³)	Relative density (%) [*]
A1	1400	2.3	6.5	98
A2		2.3	6.3	94
A3		2.4	6.0	90
B1	1450	2.3	6.3	94
B2		2.2	6.0	90
B3		1.9	5.9	89

^{*}Referred to a density of 6.68 g cm⁻³ JCPDS, card numbers 98-0080

the content of Ba and the sintering temperature. The lower densification obtained was 89% for sample B3, sintered at 1450 °C, with the highest barium content. This lower density is congruent with the SEM images, which revealed pores around 20 μm in size (Fig. 2). However, the hardness of the samples does not exhibit a direct relationship with the density. This could be associated with the material, specifically with the LSGM, *Pm-3 m* crystal structure, which seems to increase the hardness of the material sintered at 1400 °C.

Electrochemical impedance spectroscopy (EIS)

The Nyquist plots for samples evaluated at 600 and 800 °C are shown in Fig. 3. For temperatures lower than 450 °C, two arcs corresponding to the grain bulk and grain boundary resistance, respectively, appear. An inductance coil appears and keeps around 450–800 °C. In this upper range of testing, it is impossible to distinguish the relative resistance to grain bulk or grain boundary. For samples sintered at 1400 °C,

the Nyquist plot for 600 °C shows almost the same resistance for samples A1 and A3, but this is higher for A2. This should be related to many secondary phases [24], as shown in Table 3. At 800 °C, the resistance between samples A1 and A3 remains almost indistinguishable but is slightly higher for sample A3. Again, sample A2 shows the highest resistance. For samples sintered at 1450 °C, the resistance increased in the order B1, B3, and B2, respectively, for both of the measured temperatures, 600 and 800 °C.

Based on the Rietveld analysis, all samples should present similar conductivity except for sample A2, which presents a lower amount of perovskite. This was confirmed by impedance analysis. The conductivity data for all samples measured in the range of 300–800 °C are shown in Table 5. Arrhenius's plot can be seen in Fig. 4. For samples sintered at 1400 °C, the highest conductivity corresponds to sample A3 (La_{0.85}Sr_{0.075}Ba_{0.075}Ga_{0.85}Mg_{0.15}O_{3-δ}). The conductivity increased by 34% at 600 °C, which is a promising result because of increasing the efficiency of the cell at intermediate temperatures. At 800 °C, the conductivity was 3% higher for this sample. In contrast, A2 shows a reduction in the conductivity of about 0.6 times for measurements of 600 and 800 °C concerning A1. For samples sintered at 1450 °C, a barium content of 5% (B2) increased the conductivity, contrasting with the sample sintered at 1400 °C. From Table 3, this sample shows a negligible secondary phase (only 0.45% of SrLaGaO₄). This sample showed an increase of 9% at 600 °C and only 3% at 800 °C in the conductivity value in comparison with the sample without the presence of barium sintered at the same temperature. Again, the highest content of barium (B3) showed an improvement in conductivity: 22% and 25% at 600 and 800 °C, respectively. In synthesis, only the sample with a content of 5%

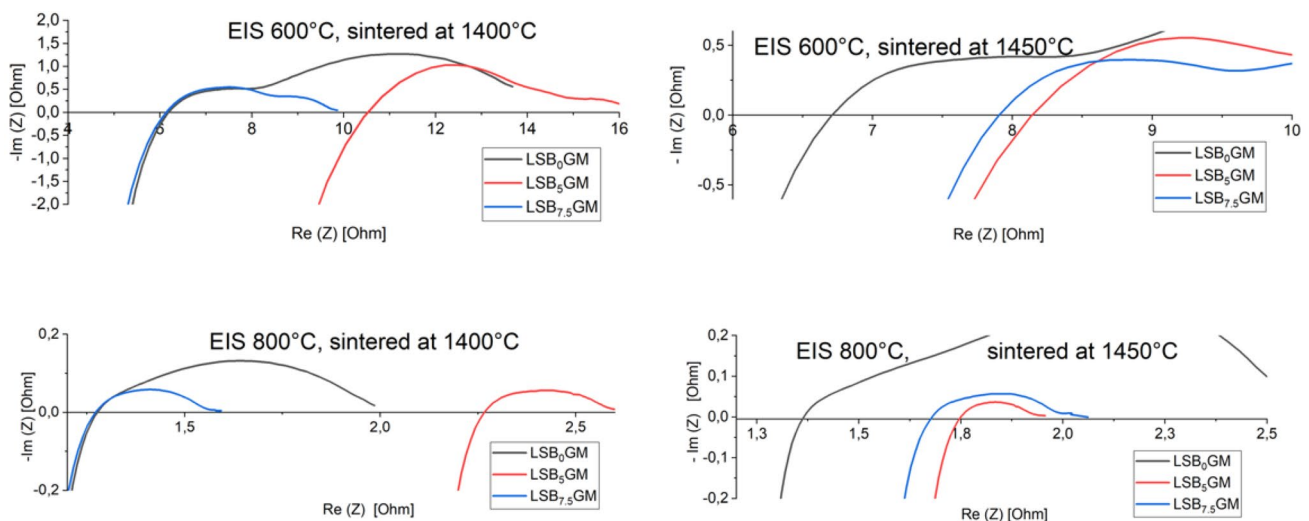
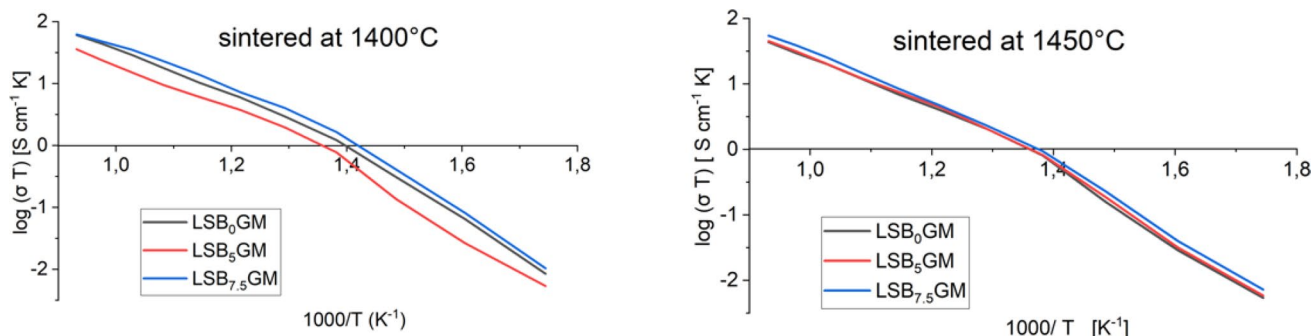


Fig. 3 EIS measured at 600 and 800 °C for LSBGM sintered at 1400 °C and 1450 °C for 6 h

Table 5 Activation energy and conductivity (S cm^{-1}) were measured at temperatures between 300 and 800 °C

Sample	300 °C	400 °C	500 °C	600 °C	700 °C	800 °C	E_{a1}^* (eV)	E_{a2}^{**} (eV)
A1	1.48×10^{-5}	4.58×10^{-4}	3.80×10^{-3}	1.18×10^{-2}	2.97×10^{-2}	5.65×10^{-2}	1.18	0.74
A2	9.39×10^{-6}	2.02×10^{-4}	2.53×10^{-3}	6.95×10^{-3}	1.56×10^{-2}	3.33×10^{-2}	1.17	0.68
A3	1.82×10^{-5}	6.10×10^{-4}	5.20×10^{-3}	1.58×10^{-2}	3.63×10^{-2}	5.82×10^{-2}	1.20	0.70
B1	9.41×10^{-6}	2.34×10^{-4}	2.60×10^{-3}	7.93×10^{-3}	2.05×10^{-2}	4.05×10^{-2}	1.19	0.75
B2	1.02×10^{-5}	2.78×10^{-4}	2.59×10^{-3}	8.65×10^{-3}	2.09×10^{-2}	4.18×10^{-2}	1.26	0.76
B3	1.26×10^{-5}	3.39×10^{-4}	2.91×10^{-3}	9.67×10^{-3}	2.62×10^{-2}	5.08×10^{-2}	1.17	0.78

*300–450 °C and **450–800 °C

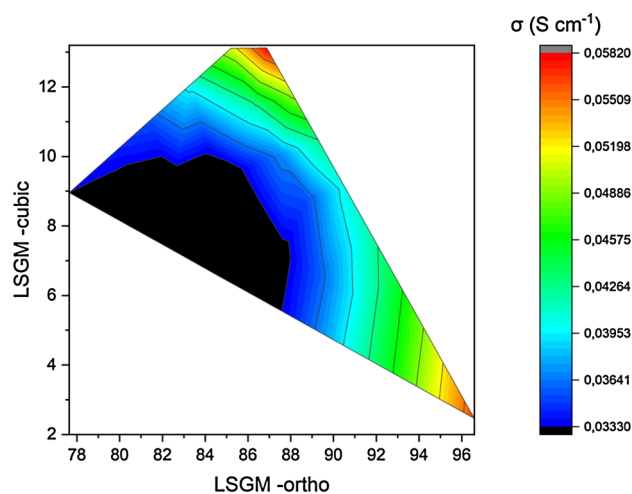
**Fig. 4** Arrhenius plots from conductivity measurements

barium increased the conductivity when the sintering temperature increased from 1400 to 1450 °C. Thus, the best conductivity was demonstrated for sample A3 (7.5% barium content) sintered at 1400 °C, while the worst conductivity was demonstrated for A2 (5% barium content) at the same temperature. It is worth noting that, from the literature, very different values have been reported. Different size samples could explain such variations. For example, Huang & Petric [14] reported 0.121 S cm^{-1} at 800 °C, while Singh & Singh [21] reported a conductivity of 0.056 S cm^{-1} at 800 °C for $\text{La}_{0.9}\text{Sr}_{0.1}\text{Ga}_{0.8}\text{Mg}_{0.2}\text{O}_{3-\delta}$ at 600 °C.

A contour diagram shows the relationships between the cubic and orthorhombic phases and the conductivity of the sample at 800 °C (Fig. 5). Also, a relationship between these phases and conductivity σ was found by linear regression to data from Tables 3–5. Equation 2 shows this relationship, where F_1 and F_2 correspond to the orthorhombic and cubic phase content, respectively.

$$\sigma = -1.86848 \times 10^{-1} + 2.03580 \times 10^{-2} \times F_1 - 1.78706 \times 10^{-4} \times F_1^2 - 1.35871 \times 10^{-1} \times F_2 + 1.90081 \times 10^{-3} \times F_2^2 + 1.12352 \times 10^{-3} \times F_1 \times F_2$$

$$R^2 = 100\% \quad (2)$$

**Fig. 5** Contour diagram for conductivity at 800 °C as a function of cubic and orthorhombic structure

Finally, the activation energy (E_a) was calculated from the Arrhenius plot. Normally, a slope change is seen in the plot, often associated with a thermal change in the internal structure, which allows the re-accommodation of the atoms, thus allowing better ionic conduction over a certain temperature [25]. In this study, the temperature was around 450–500 °C, but no phase identification at such a temperature was made

due to equipment restrictions. Data are shown in Table 5. The average E_a for the lower range was 1.2 eV, while for the upper range, it was 0.74 eV. Literature shows average values around 1.0–1.1 eV [9].

Conclusion

Different concentrations of barium were introduced into an LSGM electrolyte prepared by a fast combustion method starting from nitrate salts. The coexistence of the orthorhombic and cubic phases of LSGM was found in all samples. The combination of them could directly affect the final conductivity, as shown by a correlation found in the study. Furthermore, sintered samples at 1400 °C/6 h with 7.5% barium increased the electrolyte conductivity at 600 °C by 34% ($\text{La}_{0.85}\text{Sr}_{0.075}\text{Ba}_{0.075}\text{Ga}_{0.85}\text{Mg}_{0.15}\text{O}_{3-\delta}$; σ : 0.016 S cm^{-1}). Conductivities for samples sintered at 1450 °C were lower than those at 1400 °C, except for the sample with a 5% barium content. Finally, the conductivities were within the literature range. Thus, this method is suitable for improving the performance of LSGM electrolytes at intermediate temperatures when barium is used as a co-dopant.

Acknowledgments The authors acknowledge the financial support of FONDECYT (ANID) Project No.:1181703. Government of Chile. The authors thank Mónica Uribe from Instituto de Geología Aplicada. UDEC; the Centro de Microscopía Avanzada. CMA BIO-BIO. Proyecto PIA-ANID ECM-12 for their contribution to this work.

Funding This work was funded by the National Agency for Research and Development (ANID) / Scholarship Program/DOCTORADO NACIONAL/21202168.

Data availability The datasets generated during and/or analyzed during the current study are available from the corresponding author on reasonable request.

Declarations

Conflict of interest On behalf of all authors, the corresponding author states that there is no conflict of interest.

References

1. NOAA, *Earth system research laboratory* (NOAA, 2022)
2. A. Dicks, D. Rand, *Fuel cell systems explained* (John Wiley & Sons Ltd, 2018)
3. L. Blum, R. Deja, R. Peters, D. Stolten, Comparison of efficiencies of low, mean and high temperature fuel cell Systems. *Int. J. Hydrogen Energy* **36**(17), 11056–11067 (2011). <https://doi.org/10.1016/j.ijhydene.2011.05.122>
4. T. Ishihara, H. Matsuda, Y. Takita, Doped LaGaO₃ perovskite type oxide as a new oxide ionic conductor. *In J. Am. Chem. Soc* **116**, 3801 (1994)
5. T. Ishihara, *Perovskite oxide for solid oxide fuel cells* (Springer, 2009)
6. P.S. Cho, S.Y. Park, Y.H. Cho, S.J. Kim, Y.C. Kang, T. Mori, J.H. Lee, Preparation of LSGM powders for low temperature sintering. *Solid State Ionics* **180**(11–13), 788–791 (2009). <https://doi.org/10.1016/j.ssi.2008.12.040>
7. T. Ishihara, Development of new fast oxide ion conductor and application for intermediate temperature solid oxide fuel cells. *Bull. Chem. Soc. Japan* **79**(8), 1155–1166 (2006). <https://doi.org/10.1246/bcsj.79.1155>
8. K. Huang, J.B. Goodenough, *Solid oxide fuel cell technology: principles performance and operations* (CRC Press, 2009)
9. R.C. Biswal, K. Biswas, Novel way of phase stability of LSGM and its conductivity enhancement. *Int. J. Hydrogen Energy* **40**(1), 509–518 (2015). <https://doi.org/10.1016/j.ijhydene.2014.10.099>
10. R.K. Raghvendra Singh, P. Singh, Electrical properties of Ba doped LSGM for electrolyte material of solid oxide fuel cells. *AIP Conf. Proc.* **1512**(2012), 976–977 (2013). <https://doi.org/10.1063/1.4791368>
11. M.M. Guenter, M. Lerch, H. Boysen, D. Toebbens, E. Suard, C. Baehtz, Combined neutron and synchrotron X-ray diffraction study of Sr/Mg-doped lanthanum gallates up to high temperatures. *J. Phys. Chem. Solids* **67**(8), 1754–1768 (2006). <https://doi.org/10.1016/j.jpcs.2006.04.001>
12. Y. Wang, X. Liu, G.D. Yao, R.C. Liebermann, M. Dudley, High temperature transmission electron microscopy and X-ray diffraction studies of twinning and the phase transition at 145 d°C in LaGaO₃. *Mater. Sci. Eng. A* **132**, 13–21 (1991)
13. K. Huang, R. Tichy, J. Goodenough, Superior perovskite oxide-ion conductor; strontium-and magnesium-doped LaGaO₃: I, phase relationships and electrical properties. *J. Am. Ceram. Soc.* **81**(10), 2565–2575 (1998)
14. P. Huang, A. Petric, Superior oxygen ion conductivity of lanthanum gallate doped with strontium and magnesium. *Electrochem. Soc.* **143**(5), 1644 (1996)
15. Ç. Öncel, M. Gulgun, Chemical synthesis of mixed oxide powders for solid oxide fuel cell (SOFC) electrolyte and electrodes, in *Assessment of hydrogen energy for sustainable development*. (Springer, 2007), pp.147–159
16. D. Kioupis, A. Gaki, G. Kakali, Wet chemical synthesis of La_{1-x}Sr_xGa_{0.8}Mg_{0.2}O_{3-σ} (x=0.1, 0.2, 0.3) powders. *Mater. Sci. Forum* **636–637**, 908–913 (2010). <https://doi.org/10.4028/www.scientific.net/MSF.636-637.908>
17. M. Kakihana, Invited review “Sol-Gel” preparation of high temperature superconducting oxides*. *J. Sol-Gel. Sci. Technol.* **6**, 7–55 (1996)
18. M. Pechini, *Method of preparing lead and alkaline earth titanates and niobates and coating method using the same to form a capacitor* (Sprague Electric Co, 1967)
19. P. Majewski, M. Rozumek, C.A. Tas, F. Aldinger, Processing of (La, Sr)(Ga, Mg)O₃ solid electrolyte. *J. Electroceram.* **8**, 65–73 (2002)
20. E. Djurado, M. Labeaub, Second phases in doped lanthanum gallate perovskites. *J. Euro. Ceram. Soc.* **18**, 1397–1404 (1998)
21. R.K. Singh, P. Singh, Electrical conductivity of barium substituted LSGM electrolyte materials for IT-SOFC. *Solid State Ionics* **262**, 428–432 (2014). <https://doi.org/10.1016/j.ssi.2014.01.044>
22. M. Morales, J.J. Roa, J. Tartaj, M. Segarra, A review of doped lanthanum gallates as electrolytes for intermediate temperature solid oxides fuel cells: from materials processing to electrical and thermo-mechanical properties. *J Euro Ceram Soc* **36**(1), 1–16 (2016). <https://doi.org/10.1016/j.jeurceramsoc.2015.09.025>
23. M. Morales, J.J. Roa, J.M. Perez-Falcón, A. Moure, J. Tartaj, F. Espiell, M. Segarra, Correlation between electrical and mechanical properties in La_{1-x}Sr_xGa_{1-y}Mg_yO_{3-δ} ceramics used as

- electrolytes for solid oxide fuel cells. *J. Power Sources* **246**, 918–925 (2014). <https://doi.org/10.1016/j.jpowsour.2013.08.028>
24. L. Cong, T. He, Y. Ji, P. Guan, Y. Huang, W. Su, S. synthesis and characterization of IT-electrolyte with perovskite structure La Sr Ga Mg O by glycine-nitrate combustion method. *J. Alloys Compd.* **348**, 325 (2003)
25. L. Vasylechko, A. Senyshyn, Y. Pivak, M. Berkowske, V. Vashook, H. Ullmann, C. Bähz, U. Bismayer, LSGM single crystals: crystal structure, thermal expansion, phase transitions and conductivity, in *Mixed ionic electronic conducting perovskites for advanced energy systems*. (Springer, 2004), pp.231–237

Publisher's note Springer Nature remains neutral with regard to jurisdictional claims in published maps and institutional affiliations.

Springer Nature or its licensor (e.g. a society or other partner) holds exclusive rights to this article under a publishing agreement with the author(s) or other rightsholder(s); author self-archiving of the accepted manuscript version of this article is solely governed by the terms of such publishing agreement and applicable law.